Dyes and Pigments 103 (2014) 191–201

Contents lists available at ScienceDirect

Dyes and Pigments

journal homepage: www.elsevier.com/locate/dyepig

Two-photon fluorescence imaging of RNA in nucleoli and cytoplasm in living cells based on low molecular weight probes

Yong Liu [a,1], Weijia Zhang [a,1], Yuming Sun [b], Guofen Song [a], Fang Miao [a], Fuqiang Guo [a], Minggang Tian [a], Xiaoqiang Yu [a,*], Jing Zhi Sun [c,**]

[a] Center of Bio & Micro/Nano Functional Materials, State Key Laboratory of Crystal Materials, Shandong University, Jinan 250100, PR China
[b] School of Information Science and Engineering, Shandong University, Jinan 250100, PR China
[c] MoE Key Laboratory of Macromolecule Synthesis and Functionalization, Department of Polymer Science and Engineering, Institute of Biomedical Macromolecules, Zhejiang University, Hangzhou 310027, PR China

ARTICLE INFO

Article history:
Received 21 August 2013
Received in revised form
28 November 2013
Accepted 6 December 2013
Available online 21 December 2013

Keywords:
Ribonucleic acid
Probes
Living cells
Two-photon fluorescence
Counterstain compatibility
Low molecular weight

ABSTRACT

Two low molecular weight, indole-based, mono-cationic probes, were designed and synthesized. According to their spectral response to ribonucleic acid *in vitro* and direct fluorescence imaging in living cell lines, the two compounds were identified as ribonucleic acid-selective fluorescent turn-on probes with large two-photon excited fluorescence action absorption cross-sections when binding to ribonucleic acid. Moreover, both dyes with good membrane permeability have been successfully used to image ribonucleic acid in nucleoli and cytoplasm in living cells by confocal and two-photon fluorescence microscopy. Furthermore, the dyes possess good counterstain compatibility with Hoechst 33342, important deoxyribonucleic acid-staining dyes for ribonucleic acid–deoxyribonucleic acid colocalization.

1. Introduction

In-vivo, fluorescent imaging of ribonucleic acid (RNA) in nucleoli and cytoplasm is of great significance in biochemistry and biomedicine [1,2]. For example, Knowles et al., used nucleic acid (NA)stain SYTO 14 to visualize the translocation of endogenous RNA in living cells, and they found that labeled RNA was distributed nonrandomly as discrete granules in the neuronal processes [3]. Fluorescent imaging of RNA in parasites increases parasite detection, improves the spatial and temporal resolution of the parasite under drug treatments, and resolves the problems of morphological changing in an individual cell [4]. Previously, several classes of molecular probes have been developed for RNA detection in living cells, including (a) oligodeoxyribonucleotides (ODN) (Chart. S1) probes [5]; (b) linear fluorescence resonance energy transfer (FRET) probes [6]; (c) dual-labeled oligonucleotide hairpin probes (e.g., molecular beacons) [7]; (d) dual FRET molecular beacons [8]; (e) autoligation probes [9]; and (f) probes using fluorescent proteins as reporters [10,11]. However, because most of the RNA fluorescent probes have no membrane-permeability, they have to be injected into a target living cell in a typical *in-vivo* fluorescent imaging process [12–14]. Such a microinjection technology is destructive to living cells and may cause biological malfunctions [12,15], it is necessary to develop a low-molecular-weight fluorescent probe for imaging RNA in living cells. Even though there are many commercially available dyes with membrane-permeability for various organelles such as the nucleus [16] and mitochondria [17], preparation of RNA fluorescent probes with membrane permeability is still a challenge. Some of the facts that restricted its development include the diminished affinity to RNA than to double-stranded deoxyribonucleic acid (DNA) [18], the non-specificity in binding with proteins due to the hydrophobicity of probe molecules. Moreover, there is limited knowledge of the interaction mechanisms between RNA and fluorescent probes, including outside, groove and intercalative binding [19], compared with the wealth of papers on DNA biosensors. All increased the difficulties to develop an RNA biosensor, which also promotes the demand for a library of compounds. Li and coworkers screened a large combinatorial library of 1336 fluorescent styryl molecules but

* Corresponding author. Tel.: +86 0531 88366418; fax: +86 0531 88364263.
** Corresponding author. Tel./fax: +86 0571 87953734.
E-mail addresses: yuxq@sdu.edu.cn (X. Yu), sunjz@zju.edu.cn (J.Z. Sun).
[1] Liu and Zhang made equal contributions to this work.

0143-7208/$ – see front matter © 2013 Elsevier Ltd. All rights reserved.
http://dx.doi.org/10.1016/j.dyepig.2013.12.005

ultimately obtained only three RNA probes [20]. In another work just three dyes displaying high affinities to RNA were sifted from 125 fluorescent molecules [4]. Even though Molecular Probes Co. offers a commercially available RNA probe "SYTO RNA-Select" [21] for RNA imaging in living cells, its chemical structure has not been described.

Two-photon fluorescence microscopy (TPM) has advantages over traditional techniques such as lower photodamage, reduced photobleaching, higher detection sensitivity, as well as diminished image distortion [22–27]. TPM has an intrinsically high axial resolution without the need of a confocal pinhole in the detection path. Also the technique will reduce cell damage by using either longer wavelength excitation light, which avoids damaging ultraviolet (UV) [28], or blue excitation light. It also reduced out-of-focus irradiations [29,30]. Therefore, TPM can be used for repetitive imaging of living cells without severely damaging the cellular vitality. The fast development of two-photon excited fluorescence (TPEF) probes to different targets in living cells has attracted a lot of attention and many researchers [31–34], including us [35], have contributed to this area. Amongst all of these, the only one on live-cell RNA TPEF probes was given by Ohulchanskyy et al., who found that the conventional NA dye 4-((1-methylbenzothiazolyliliden-2) methyl)-1,2,6-trimethylpyridinium perchlorate (cyan 40) (Chart. S2) could be used to image RNA in nucleoli in TPM [36]. However, its two-photon excited fluorescence action absorption cross-sections ($\Phi \times \delta$), a crucial parameter for TPEF probes, was not given. Given the limited number of suitable dyes we were keen to explore new RNA-selective biosensors that can be used for both confocal microscopy and TPM in living cells.

In our previous work, we have focused on small-molecule probes, carbazole derivatives, for selective imaging NA, cysteine and lysosome in live-cells and deep tissues [35,37,38]. These dyes possesses large $\Phi \times \delta$, thus they can luminescence more intensely under the some incident power. Despite the numerous desirable properties of small-molecule NA probes have been designed by us [37], many of them work well with DNA in plant tissue but are not suitable for RNA TP imaging in living human cells. Among them, possessing V-shaped conjugated structures inspired us to survey RNA markers, especially TPEF live-cell RNA sensors among various cationic salts with the particular chemical structure. The results indicate that this idea should be rational. In this ongoing study we synthesized and examined V-shape structures, namely 3,5-bis((*E*)-2-(pyridin-4-yl)vinyl)-1*H*-indole monoiodides (**INR1**/**INR2**) (Scheme 1).

2. Material and methods

2.1. Material

All chemicals used are of analytical grade, and 4-picoline, 1-iodobutane, 1-iodohexane and 5-Bromo-1*H*-indole-3-carbal dehyde were purchased from Sinopharm Chemical Reagent Co., Ltd (Shanghai, China). Palladium (II) acetate and tri-*o*-tolylphosphine were purchased from **J&K Chemical** (Beijing, China). Tris and PBS were purchased from Seikagaku Corporation (Japan). The solvents used in the spectral measurement are of chromatographic grade. The double-stranded DNA-specific dye 4′,6-diamidino-2-phenylindole (DAPI)/Hoechst 33342 and SYTO RNA-Select were purchased from Molecular Probes. Calf thymus DNA and torula yeast RNA, which were used as the model of DNA and RNA, and ribonuclease A (RNase) were obtained from Sigma. Spectroscopic measurements of were performed in acetonitrile/Tris–HCl buffer solution (tris: 10 mM, KCl: 100 mM) with pH 7.2. TLC analyses were performed on silica gel plates and column chromatography was conducted over silica gel (mesh 200–300), both of which were obtained from Qingdao Ocean Chemicals.

2.2. Measurements

Nuclear magnetic resonance spectra (^{1}H and ^{13}C) were obtained on a Bruker Avanace 300/400 spectrometer. The HRMS spectra were recorded on Agilent Technologies 6510 Q-TOF LC/MS or ThermoFisher LCQ FLEET. The elemental analyses were performed on a Vario EI III instrument. The UV–visible–near-IR absorption spectra of dilute solutions were recorded on a Cary 50 spectrophotometer using a quartz cuvette having 1 cm path length. One-photon fluorescence spectra were obtained on a HITACHI F-2700 spectrofluorimeter equipped with a 450-W Xe lamp. Two-photon fluorescence spectra were recorded on a SpectroPro300i and the pump laser beam comes from a mode-locked Ti: sapphire laser system at the pulse duration of 200 fs, with a repetition rate of 76 MHz (Coherent Mira900-D). Confocal microscopic photos of photostability were obtained with Carl Zeiss Microscopy LSM780, The confocal microscopic image and differential interference contrast (DIC) image were taken with a 488 nm laser, CD Spectrometer Jasco J-810.

Wide-field fluorescence microscopy images were acquired with an Olympus IX71 inverted microscope coupling with a CCD and display controller software. The fluorescence of four dyes and DAPI/Hoechst 33342 were excited and collected through U-MNIBA3 and U-MWU2, respectively. The confocal microscopic image and differential interference contrast (DIC) image were taken with a 488 nm Arion laser. Fluorescence of **INR1**/**INR2** were collected with a beam splitter DM570 and BA510-540 nm bandpass emission filter combination. All of TPM microscopic photos were obtained with Olympus FV 300 Laser Confocal System with a 60× water objective (N.A. = 1.25) and photomultiplier tubes and Ti: sapphire laser (Coherent) was used to excite the specimen at 800 nm. The total power provided by laser source can be maintained stable and the incident power was examined with Power Monitor (Coherent) directly. A multiphoton emission filter (FF01-750; Semrock) was used to block the IR laser.

TPA cross-sections have been measured using the two-photon induced fluorescence method [40]. Fluorescein (pH = 13, cyan

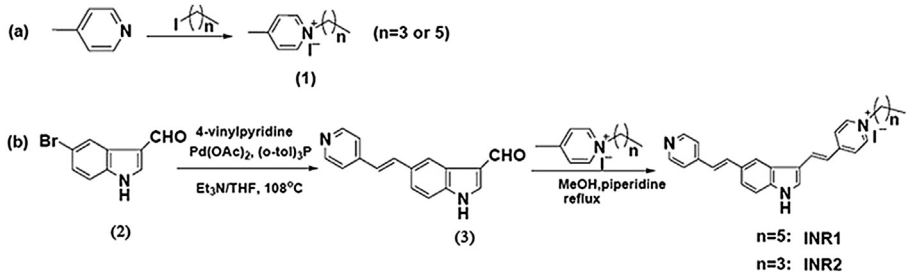

Scheme 1. The synthetic routes to **INR1**/**INR2**.

diamond) in aqueous NaOH was used as the standard, whose two-photon properties have been well characterized in the literature [41], and thus cross-sections can be calculated by means of equation (1)

$$\delta_s = \delta_r \frac{\Phi_r}{\Phi_s}\frac{c_r}{c_s}\frac{n_r}{n_s}\frac{F_s}{F_r} \quad (1)$$

where the subscripts *s* and *r* refer to the sample and the reference materials, respectively. δ is the two-photon absorption (TPA) cross sectional value, *c* is the concentration of the solution, *n* is the refractive index of the solution, *F* is the two-photon excited fluorescence integral intensity and Φ is the fluorescence quantum yield. TPA quantum yield measurement is quite difficult compared to the well-established quantum yield measurement of one-photon fluorescence. So, one might suppose that two quantum yields are coincidental.

2.3. Synthesis and characterization

2.3.1. N-(2-butyl/hexyl)-4-methylpyridinium iodide (**1**)

4-picoline (4.65 g, 0.05 mol) and 1-iodobutane (11.04 g, 0.06 mol) or 1-iodohexane (12.72 g, 0.06 mol) were mixed and stirred for 4 h, thereafter heated under refluxed for 2 h. After cooling and filtrating, the final products were washed with ether. The title product was obtained as a red viscous liquid.

N-(2-butyl)-4-methylpyridinium iodide ($n = 3$): The yield: 13.16 g (95.0%), boiling point (bp) (760 mmHg): 214–215 °C. FT-IR (KBr) γ (cm^{-1}): 2873–2933 (CH, aliphatic), 1973 (C═N); 1470–1517 (C═C, phenyl). ^{1}H NMR (DMSO-d_6, 400 MHz), δ (ppm): 8.99 (d, $J = 6.6$ Hz, 2H), 8.00 (d, $J = 6.4$ Hz, 2H), 4.57 (t, $J = 7.4$ Hz, 2H), 2.61 (s, 3H), 1.86 (m, 2H), 1.26 (m, 2H), 0.89 (t, $J = 7.4$ Hz, 3H). ^{13}C NMR (400 MHz, DMSO-d_6), δ (ppm): 159.19, 144.07, 128.81, 60.02, 32.99, 22.01, 19.12, 13.81. HRMS: *m*/*z* ($C_{10}H_{16}IN$), found: 150.1309 $[M - I]^+$.

N-(2-hexyl)-4-methylpyridinium iodide ($n = 5$): The yield: 13.72 g (90.0%), bp (760 mmHg): 215–216 °C. FT-IR (KBr) γ (cm^{-1}): 2857–2952 (CH, aliphatic), 1973 (C═N); 1469–1517 (C═C, phenyl). ^{1}H NMR (DMSO-d_6, 400 MHz), δ (ppm): 9.05 (d, $J = 6.6$ Hz, 2H), 8.05 (d, $J = 6.4$ Hz, 2H), 4.60 (t, $J = 7.4$ Hz, 2H), 2.64 (s, 3H), 1.92 (m, 2H), 1.28 (s, 6H), 0.86 (t, $J = 6.8$ Hz, 3H). ^{13}C NMR (400 MHz, DMSO-d_6), δ (ppm): 159.15, 144.11, 128.81, 60.21, 31.03, 30.98, 25.40, 22.30, 21.98, 14.28. HRMS: *m*/*z* ($C_{12}H_{20}IN$), found: 178.1579 $[M - I]^+$.

2.3.2. Synthesis of (E)-5-(2-(pyridin-4-yl) vinyl)-1H-indole-3-carbaldehyde (**3**)

5-Bromo-1*H*-indole-3-carbaldehyde **2** (1.12 g, 5.00 mmol) was added to a high pressure tube with a mixture of palladium(II) acetate (0.11 g, 0.50 mmol), tri-*o*-tolylphosphine (0.46 g, 1.50 mmol) and then to which was added the solvent pair triethylamine (14 mL, 0.10 mol)/tetrahydrofuran (42 mL, 0.52 mol) and 4-vinylpyridine (2 mL, 0.02 mol). The tube was sealed after bubbling for 15 min with nitrogen. After keeping the system under ~108 °C for three days, the precipitate was collected and washed with water and dichloromethane. The title product was obtained as a yellow solid. The yield: 0.62 g (50.0%), melting point (mp): 285–286 °C. FT-IR (KBr) γ (cm^{-1}): 3247 (N–H), 3022 (Ar–H), 1640 (–C═O), 1596–1641 (C═C), 958 (═C–H). ^{1}H NMR (DMSO-d_6, 300 MHz), δ (ppm): 12.21 (s, 1H), 9.97 (s, 1H), 8.53 (d, $J = 6.0$ Hz, 2H), 8.33 (d, $J = 12.9$ Hz, 2H), 7.70 (d, $J = 16.5$ Hz, 1H), 7.64 (dd, $J = 8.4$ Hz, 1.5 Hz, 1H), 7.60 (d, $J = 6.0$ Hz, 2H), 7.54 (d, $J = 8.4$ Hz, 1H), 7.19 (d, $J = 16.2$ Hz, 1H). ^{13}C NMR (400 MHz, DMSO-d_6), δ (ppm): 185.52, 150.40, 145.13, 139.69, 137.74, 134.58, 131.03, 125.01, 124.47, 122.86, 121.19, 120.93, 118.87, 113.36. HRMS: *m*/*z* ($C_{16}H_{12}N_2O$), found: 249.1041 $[M + H]^+$.

2.3.3. Synthesis of ***INR1***/***INR2***

The condensation between **3** (0.36 g, 1.45 mmol) and *N*-(2-hexyl)-4-methylpyridinium iodide (0.49 g, 1.57 mmol) or *N*-(2-butyl)-4-methylpyridinium iodide (0.43 g, 1.57 mmol) happened in methanol with about four drops of piperidine. The mixture was stirred at 70 °C for 4 h and then a precipitate was formed. This precipitate was filtered and washed with dichloromethane and little methanol as a red powder, which was then recrystallized from methanol twice. The title product was obtained as a red solid.

INR1 ($n = 5$): The yield: 0.50 g (68%), mp: 280–281 °C. FT-IR (KBr) γ (cm^{-1}): 3128 (N–H), 2927 (CH, aliphatic), 1593 (C═C), 968 (═C–H). ^{1}H NMR (400 MHz, DMSO-d_6), δ (ppm): 12.05 (d, $J = 2.0$ Hz, 1H), 8.81 (d, $J = 6.8$ Hz, 2H), 8.58 (d, $J = 5.5$ Hz, 2H), 8.40 (s, 1H), 8.28 (d, $J = 16.0$ Hz, 1H), 8.17 (d, $J = 6.8$ Hz, 2H), 8.00 (d, $J = 2.8$ Hz, 1H), 7.61 (m, 5H), 7.34 (dd, $J = 23.3$, 16.3 Hz, 2H), 4.43 (t, $J = 7.3$ Hz, 2H), 1.91 (m, 2H), 1.31 (s, 6H), 0.87 (t, $J = 6.7$ Hz, 3H). ^{13}C NMR (300 MHz, DMSO-d_6), δ (ppm): 155.36, 150.49, 146.28, 144.37, 138.73, 137.05, 135.69, 133.82, 130.58, 126.33, 124.66, 123.00, 121.66, 121.07, 118.27, 115.01, 114.00, 60.05, 31.50, 31.30, 26.07, 22.83, 14.77. HRMS: *m*/*z* ($C_{28}H_{30}IN_3$), found: 408.2465$[M - I]^+$. Anal. calcd. for $C_{28}H_{30}IN_3$ (%): C 62.81, H 5.65, N 7.81; found: C 62.60, H 5.41, N 7.34.

INR2 ($n = 3$): The yield: 0.50 g (65%), mp: 295–296 °C. FT-IR (KBr) γ (cm^{-1}): 3146 (N–H), 3029 (Ar–H); 2962 (CH, aliphatic), 1593–1639 (C═C), 971 (═C–H). ^{1}H NMR (400 MHz, DMSO-d_6), δ (ppm): 12.06 (s, 1H), 8.82 (d, $J = 6.9$ Hz, 2H), 8.56 (d, $J = 6.0$ Hz, 2H), 8.41 (s, 1H), 8.29 (d, $J = 16.2$ Hz, 1H), 8.18 (d, $J = 6.9$ Hz, 2H), 8.00 (s, 1H), 7.71 (d, $J = 16.4$ Hz, 1H), 7.64 (dd, $J = 8.5$, 1.0 Hz, 1H), 7.57 (m, 3H), 7.38 (d, $J = 16.2$ Hz, 1H), 7.31 (d, $J = 16.4$ Hz, 1H), 4.45 (t, $J = 7.3$ Hz, 2H), 1.89 (m, 2H), 1.33 (m, 2H), 0.97 (t, $J = 6.7$ Hz, 3H). ^{13}C NMR (300 MHz, DMSO-d_6), δ (ppm): 154.87, 150.50, 145.23, 143.90, 138.20, 136.58, 134.75, 133.35, 130.14, 125.83, 124.30, 122.49, 121.06, 120.49, 117.75, 114.50, 113.51, 59.33, 32.95, 19.30, 13.86. HRMS: *m*/*z* ($C_{26}H_{26}IN_3$), found: 380.2119 $[M - I]^+$. Anal. calcd. for $C_{26}H_{26}IN_3$ (%): C 61.53, H 5.16, N 8.28; found: C 61.39, H 5.25, N 8.31.

2.4. Cell culture

Cancer cells (SiHa and HeLa) were cultured in Dulbecco's modified Eagle's medium supplemented with penicillin/streptomycin and 10% bovine calf serum in a 5% CO_2 incubator at 37 °C. Cells PC3 and MDA-MB-231 were grown in Dulbecco's modified Eagle's medium and 10% bovine calf serum in a 5% CO_2 incubator at 37 °C.

2.5. Live-cell imaging

For living cells imaging experiment of **INR1**/**INR2**, cells were incubated with 10 μM **INR1**/**INR2** in PBS (pH 7.2) for 1.5 h at 37 °C. After rinsing with PBS twice, cells were imaged immediately. **INR1**/**INR2** were dissolved in DMSO at a concentration of 1 mM and Hoechst 33342 was prepared as 1 mM aqueous solution.

For wide-field fluorescence microscopy, confocal fluorescence microscopy and TPM imaging of cells stained with **INR1**/**INR2**: Living SiHa cells were stained with 10 μM **INR1**/**INR2** for 1.5 h at ambient temperature and then imaged with fluorescence microscopy. For cells counterstain experiment with the dyes and Hoechst 33342: Living SiHa cells were stained with 10 μM dyes for 1.5 h. After rinsing with PBS twice, the same sample was stained with 5 μM Hoechst 33342 for 30 min and then imaged with wide-field fluorescence microscopy.

2.6. RNase digest test of fixed cells

Before cells digest test, cultured cells grown on glass coverslips were pretreated according to the following procedure: cells were

first fixed by 4% paraformaldehyde for 30 min and then permeabilized by 0.5% Trition X-100 for 2 min at ambient temperature. DAPI was prepared as 1 mM aqueous solution. For RNase digest test, two sets of pretreated SiHa cells were stained with 10 μM **INR1**/**INR2** for 30 min. After rinsing with PBS twice, a total 1 mL PBS (as control experiment) was added into a set of cells and 25 mg/mL DNase-Free RNase (GE) was added into the other set of cells, and then two sets of cells were incubated at 37 °C in 5% CO_2 for 2 h. After rinsing with PBS twice, both two sets of cells were imaged with wide-field fluorescence microscopy. In addition, the RNase digest test of cells stained with 1 μM DAPI was also carried out for comparison.

2.7. Cell viability evaluated by MTT assay

Viability of the cells was assayed using cell proliferation Kit I with the absorbance of 492 nm being detected using a Perkin–Elmer Victor plate reader. Five thousand cells were seeded per well in a 96-well plate. After overnight culture, various concentrations of **INR1**/**INR2** were added into the 96-well plate. After 2 h treatment, 20 μL of 3-(4,5-dimethyl-2-thiazolyl)-2,5-diphenyltetrazolium bromide (MTT) solution (5 mg/mL in phosphate buffer solution) was added into the each well. After 4 h incubation at 37 °C, 200 μL DMSO was added to dissolve the purple crystals. After 20 min incubation, the optical density readings at 492 nm were taken using a plate reader.

3. Results and discussion

3.1. Preparation of probes

INR1/**INR2** were synthesized by Knoevenagel condensation reactions between *N*-(2-butyl/hexyl)-4-methylpyridinium iodide and a substituted indole-3-carboxaldehyde using piperidine as catalyst. The intermediate **3** was obtained by Heck coupling reaction between 5-bromo-1*H*-indole-3-carbaldehyde with 4-vinylpyridine. The separated **INR1**/**INR2** were characterized by various spectroscopic methods, from which satisfactory analysis data were obtained (Supporting Information).

3.2. RNA and DNA titrations

In the absorption spectrum of **INR1** (Fig. 1), the single peak at 425 nm, appears as a double-peak (370 nm and 467 nm for RNA, 370 nm and 464 nm for DNA) when it is mixed with NA. This suggests that strong interactions between dye and NA. Fluorescence titration experiments were then performed to study the affinity of probes to RNA and DNA (Fig. 2). The fluorescence intensity of **INR1** increase significantly in the low ratio region ([NA]:[dye] < 250:1) and decrease regularly until stable ([NA]:[dye] ranges from 700:1 to 1050:1) (Fig. 2a). Furthermore, TPEF titrations of dyes were carried out at 800 nm which is an optimal output wavelength from a commercial mode-locked Ti: sapphire laser source. In the two-photon fluorescence titration, it was found that the fluorescence intensity of **INR1** increases in the presence of RNA or DNA, and that the fluorescence in the presence of RNA is stronger than that in the presence of DNA (Fig. 2b). A similar trend is observed in the one- and two-photon fluorescence of **INR2** with addition of NA (Fig. 2c and d). The dyes preferring RNA to DNA should be superior to those, such as 2,7-bis(1-hydroxyethyl-4-vinylpyridium iodine)-*N*-ethylcarbazole (2,7-9E-BHVC) (Chart. S3) [39], with identical response to RNA and to DNA for RNA-selective probes.

Two factors can be used to explain the mechanism of the light-up effect upon binding to RNA or DNA. Firstly, dyes that are in a twist intramolecular charge transfer (TICT) state whose non-radiative process quenches the fluorescence will be non-emissive; inversely, dyes for which the formation of a TICT state is restricted become brightly luminescent [42]. For indole derivatives reported here, the intramolecular charge transfer (ICT) state could occur between the electron donor of the indole moiety and the electron acceptor of the pyridinium cation. Once in water, the larger dipole moment in the excited state than that in the ground state interacts strongly with the polar solvent, which could lead to charge separation resulting in the formation of a TICT state. However, the formation of a TICT state is restricted when the dyes are protected from water in the grooves of RNA or DNA, and finally the fluorescence of the dyes will be restored. On the other hand, the weak emission of the dyes in water can be attributed to the rapid non-radiative decay that results from the torsional motion of fluorophore responsible for the low quantum yield and from collisional interactions [43]. When binding to nucleic acids, the torsional motion of vinyl groups can be restricted by the steric effect derived from the static interactions between the cationic *N*-pyridinium and the anionic phosphate of nucleic acids, thus the fluorescence intensity can increase. Their one- and two-photon fluorescence intensities are high in organic solvents and very low in tris–HCl buffer and aqueous solution (Fig. S1). The appreciable solvent effect implies that the ICT state is predominant in the photophysical behavior of **INR1**/**INR2**, which is similar to our other carbazole derivatives [44]. It is well known that the concentration-quenching effect is common for many aromatic compounds due to the formation of sandwich-shaped excimers and exciplexes aided by the collisional interactions between the aromatic molecules in the excited and ground states [45]. However, the formation of a TICT state is restricted when the dyes are protected from water in the grooves of RNA or DNA, and finally the fluorescence of dyes will be restored.

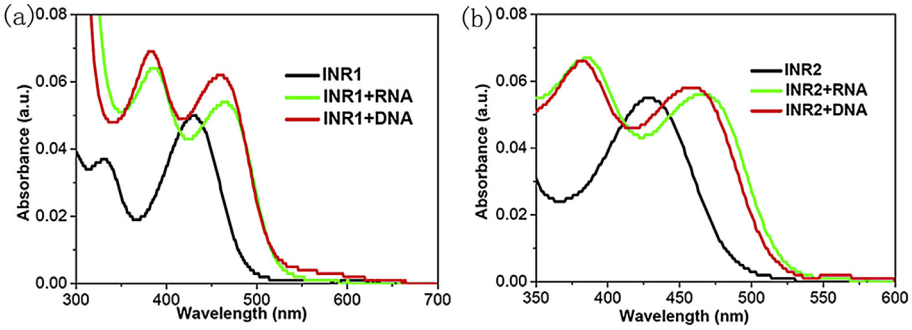

Fig. 1. The UV–vis absorption (a and b) of **INR1**/**INR2** in buffer (black), RNA (green) and DNA (red). Buffer, 10 mM Tris–HCl, 100 mM KCl, pH 7.2. Compound concentration: 2.0 μM. Ratio (phosphate of NA/dye): 1000:1 for **INR1**/**INR2**. (For interpretation of the references to color in this figure legend, the reader is referred to the web version of this article.)

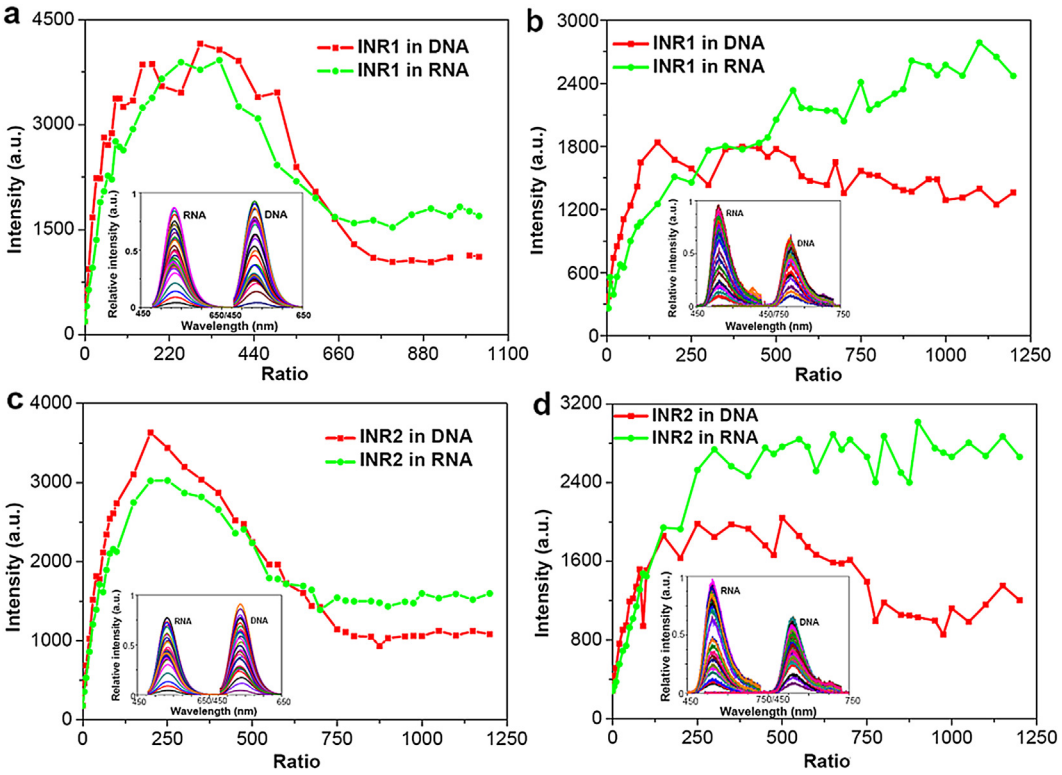

Fig. 2. One- (a and c) and two-photon (b and d) excited fluorometric titration of dyes with the addition of RNA and DNA. Each point shown in b and d has an error of 8%. Inset: the corresponding fluorescent spectra of the dyes with RNA or DNA. Compound concentration: 2.0 μM. Excitation wavelength (Ex): a and c, 465 nm; b and d, 800 nm.

3.3. Circular dichroism (CD)

To further explain the mechanism of the light-up effect upon binding to RNA, the interactions between **INR1**/**INR2** and RNA/DNA were also investigated by induced circular dichroism (ICD) spectra. As shown in Fig. 3, CD signal of RNA and DNA appear in range of 200–300 nm, and plus and minus two signals confirm spiral chain characteristics of RNA [46]. Due to induction of RNA, **INR1**/**INR2**, two compounds without optical activity, present optically activity. Moreover, there are negative Cottons effect in the electronic absorption (410–500 nm) region of **INR1** and **INR2**, implying that the electron transition easily absorbs right-circularly polarized light. Meanwhile Cotton peaks at 465 (−) nm corresponded to UV absorption peaks at 467/465 nm of **INR1**/**INR2** bound with RNA. It can be assumed that the groove binding between **INR1**/**INR2** and RNA may affect the molecular conformation and bring about an asymmetric chiral center in **INR1**/**INR2**, resulting in optical activity [47]. Compared with RNA, the induction of **INR1**/**INR2** DNA should be weaker (Fig. 3 inset). The results show that the affinity between **INR1**/**INR2** and RNA is stronger than that of DNA, thus **INR1**/**INR2** may preferentially interact with RNA within cells.

3.4. One-photon fluorescent imaging

One-photon fluorescent spectra of **INR1**/**INR2** in buffer, RNA and DNA solutions were studied before imaging. **INR1** is weakly fluorescent in the tris–HCl buffer, whereas the fluorescence intensity shows an approximately 15-fold enhancement in the presence of RNA and 6-fold in the presence of DNA (Fig. 4a). A similar trend is observed in the case of **INR2** (see Fig. 4b). This indicates that these

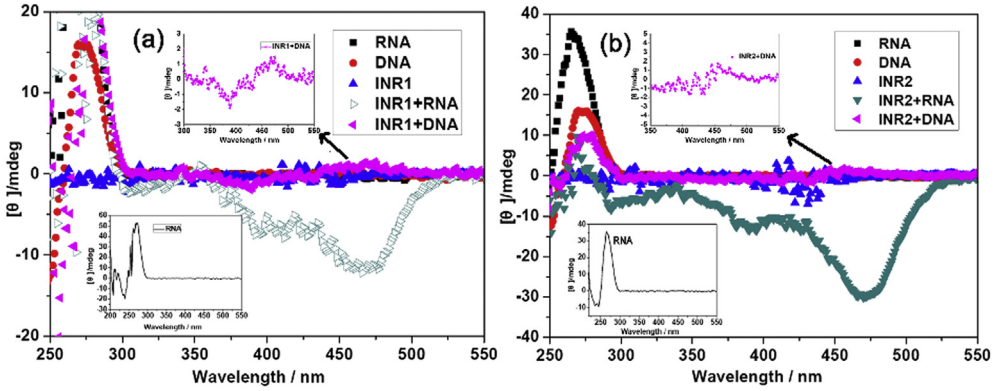

Fig. 3. (a) and (b): CD spectra of the RNA, DNA, **INR1**/**INR2**, **INR1**/**INR2** + RNA and **INR1**/**INR2** + DNA; Inset: CD spectrum of RNA and **INR1**/**INR2** + DNA. Concentration: 40 μM. Ratio (phosphate of NA/dye): 400:1 for **INR1**, 150:1for **INR2**.

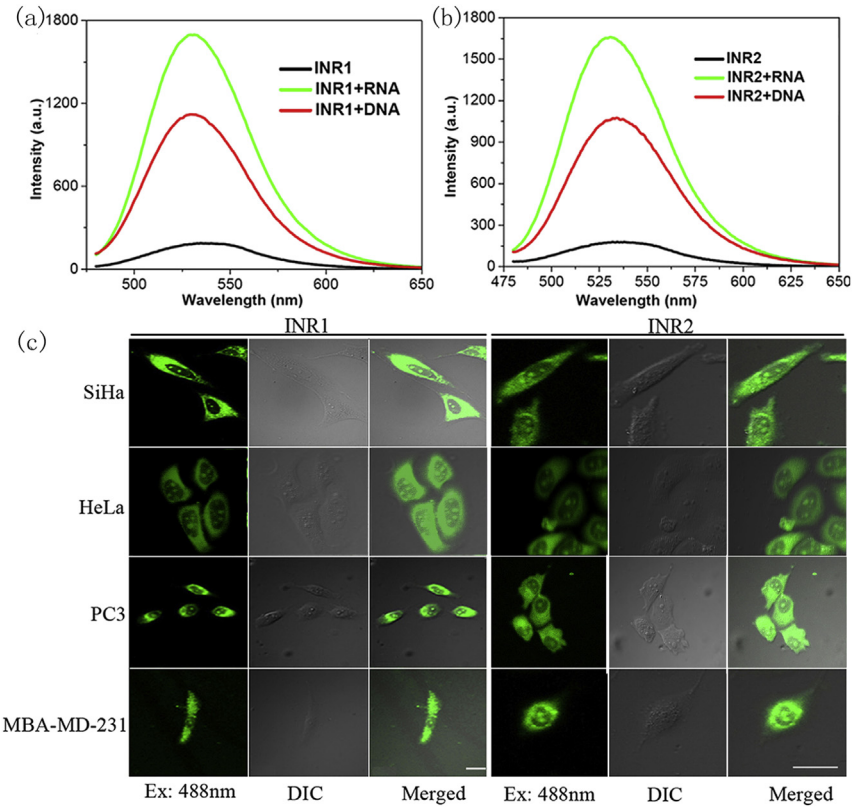

Fig. 4. One-photon excited fluorescence (a and b) spectra of **INR1**/**INR2** in buffer (black), RNA (green) and DNA (red). Buffer, 10 mM Tris–HCl, 100 mM KCl, pH 7.2. Compound concentration: 2.0 μM. Ratio (phosphate of NA/dye): 1000:1 for **INR1**/**INR2**. (c): confocal fluorescence images of live-cells (SiHa, HeLa, PC3 and MDA-MB-231) stained with 10 μM dyes for 1.5 h. Ex: 488 nm; Detection wavelength: 510–540 nm; Bar = 20 μm. (For interpretation of the references to color in this figure legend, the reader is referred to the web version of this article.)

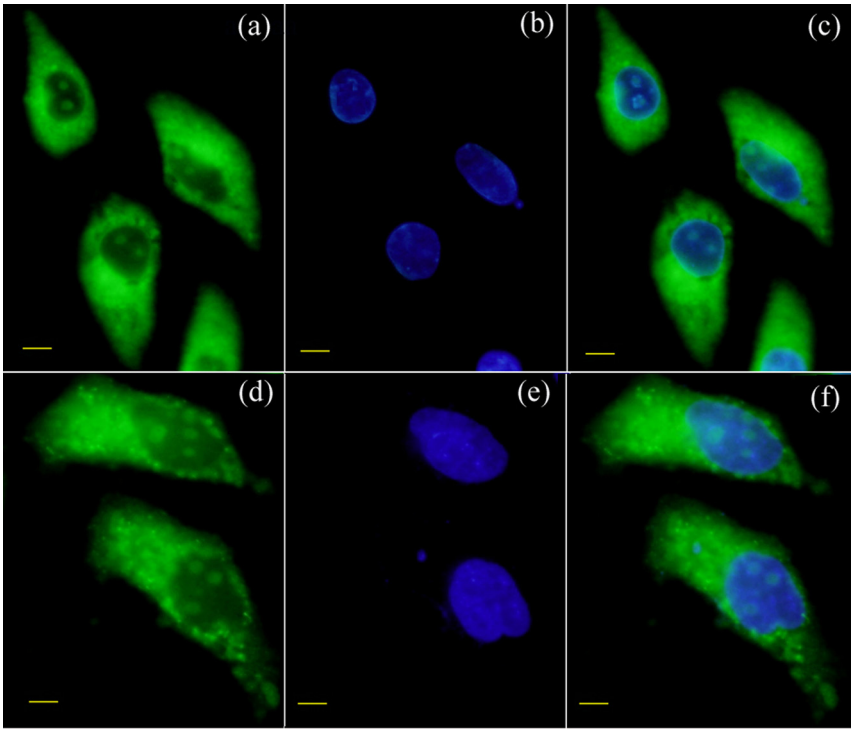

Fig. 5. Wide-field fluorescence images of SiHa cells stained with 10 μM dyes for 1.5 h followed by staining with 5 μM Hoechst 33342 for 20 min. a and d: fluorescence of dyes **INR1**/**INR2**, respectively. b and e: fluorescence of Hoechst 33342. c and f: merged picture. Ex (**INR1**/**INR2**): 460–490 nm; Detection wavelength: >510 nm; Ex (Hoechst 33342): 330–385 nm; Detection wavelength: >410 nm; Bar = 20 μm.

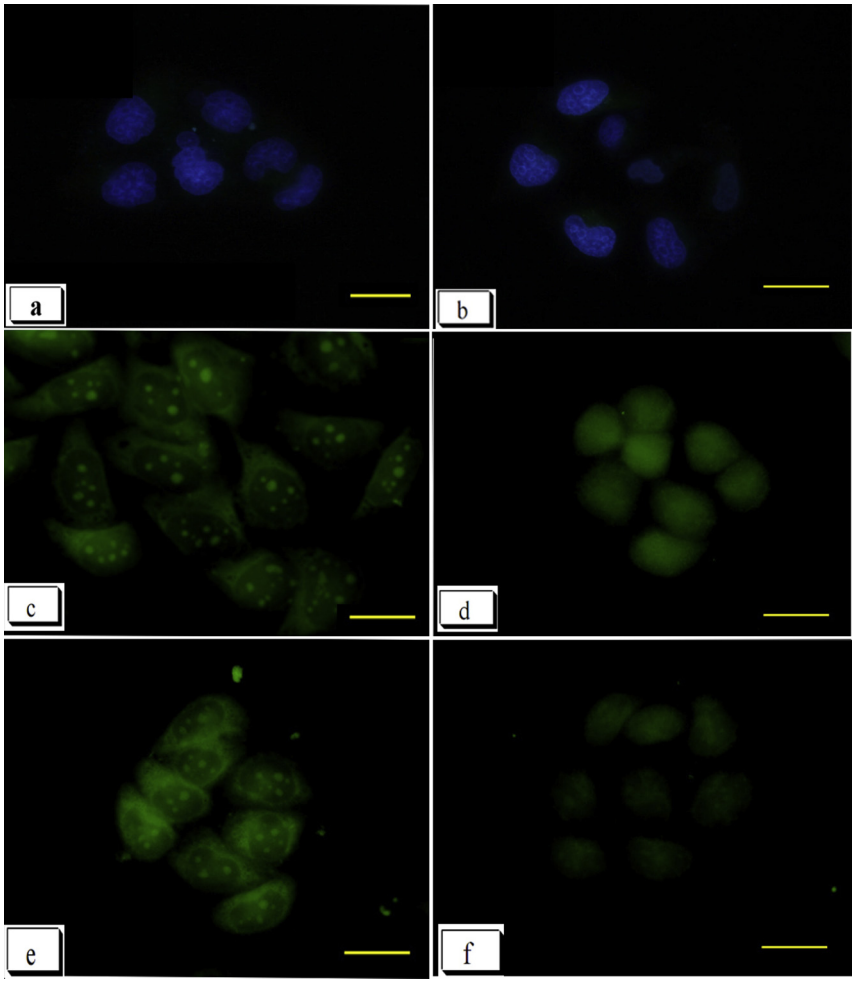

Fig. 6. The RNase digest experiment. Wide-field fluorescence imaging of SiHa cells stained with DAPI (a and b), **INR1** (c and d) and **INR2** (e and f) before (a, c and e) or after (b, d and f) treatment with RNase (30 μg/ml) for 2 h at 37 °C. Conditions: 10 μM, dyes; 1 μM, DAPI; Incubation time: 30 min. Ex (**INR1**/**INR2**): 460–490 nm, Detection wavelength: >510 nm; Ex (DAPI): 330–385 nm, Detection wavelength: >410 nm; Bar = 20 μm.

dyes have higher one-photon fluorescence responses to RNA than to DNA, and therefore have potential in imaging the RNA distribution in living cells.

The cytotoxicity of **INR1**/**INR2** were evaluated using a 3-(4,5-dimethyl-2-thiazolyl)-2,5-diphenyltetrazolium bromide (MTT) assay. The results indicate that the probes generally present low toxicity for living cell imaging (e.g., HeLa cell) under the conditions applied (Fig. S2). Four live-cell lines (SiHa, HeLa, PC3 and MDA-MB-231) were incubated. The fluorescent imaging was carried out with confocal microscopy and wide-field fluorescence microscopy (Fig. S3), using 488 nm Ar^+ laser and mercury lamp (U-MNIBA3), respectively. The differential interference contrast (DIC) images served as proof that the cells were viable throughout the imaging experiments. According to Fig. 4c, the amounts of nucleoli in SiHa and HeLa cells are more than that in PC3 and MD-MBA-231 cells and the distributions of nucleoli in the four kinds of cells are significantly different, indicating that there is diverse transcriptional activity in different cell lines. The green fluorescence mainly localizes in nucleoli, a dense region of rRNA, and cytoplasm where mRNA is likely to be present. Moreover, it is evident that the position, shape and amount of the distinguishable nucleoli labeled by **INR1**/**INR2** are consistent with the dense, dark-phase region of the nucleus in DIC photos which definitely represents nucleoli.

A good compatibility of RNA sensors with the classic DNA-staining dye Hoechst 33342 would be helpful in imaging DNA and RNA distribution simultaneously. Fig. 5 shows the counterstain result of dyes and Hoechst 33342. The green fluorescence from nucleoli and cytoplasm is easily discriminated from the nuclear zone with blue fluorescence in live SiHa cells, which indicates a good counterstain compatibility with Hoechst 33342. The characteristics of these dyes could help to image RNA distribution in relation to DNA in living cells and probably to reveal different patterns of RNA–DNA colocalization which are cell type dependent.

To further confirm the selectivity of dyes to RNA, the digest test of ribonuclease (RNase) was performed (Fig. 6), in which RNA was hydrolyzed while DNA kept intact. Fixed-permeabilized HeLa cells were used in this experiment, with DAPI (Chart. S4) in the control group. After treatment with RNase, the fluorescence in cytoplasm and nucleoli dramatically diminished and tended to redistribute to the nucleus (Fig. 6d and f) in contrast to the untreated sample (Fig. 6c and e). However, there was no apparent effect on the staining result of DAPI (Fig. 6a and b), considering that the double-stranded DNA is a more preferable target for DAPI than RNA [20]. This result indicates that **INR1**/**INR2** prefer RNA to DNA in the complex internal environment of cells.

3.5. Two-photon fluorescent imaging

The influence of DNA and RNA on their selectivity in TPEF properties was examined before imaging RNA in living cells with

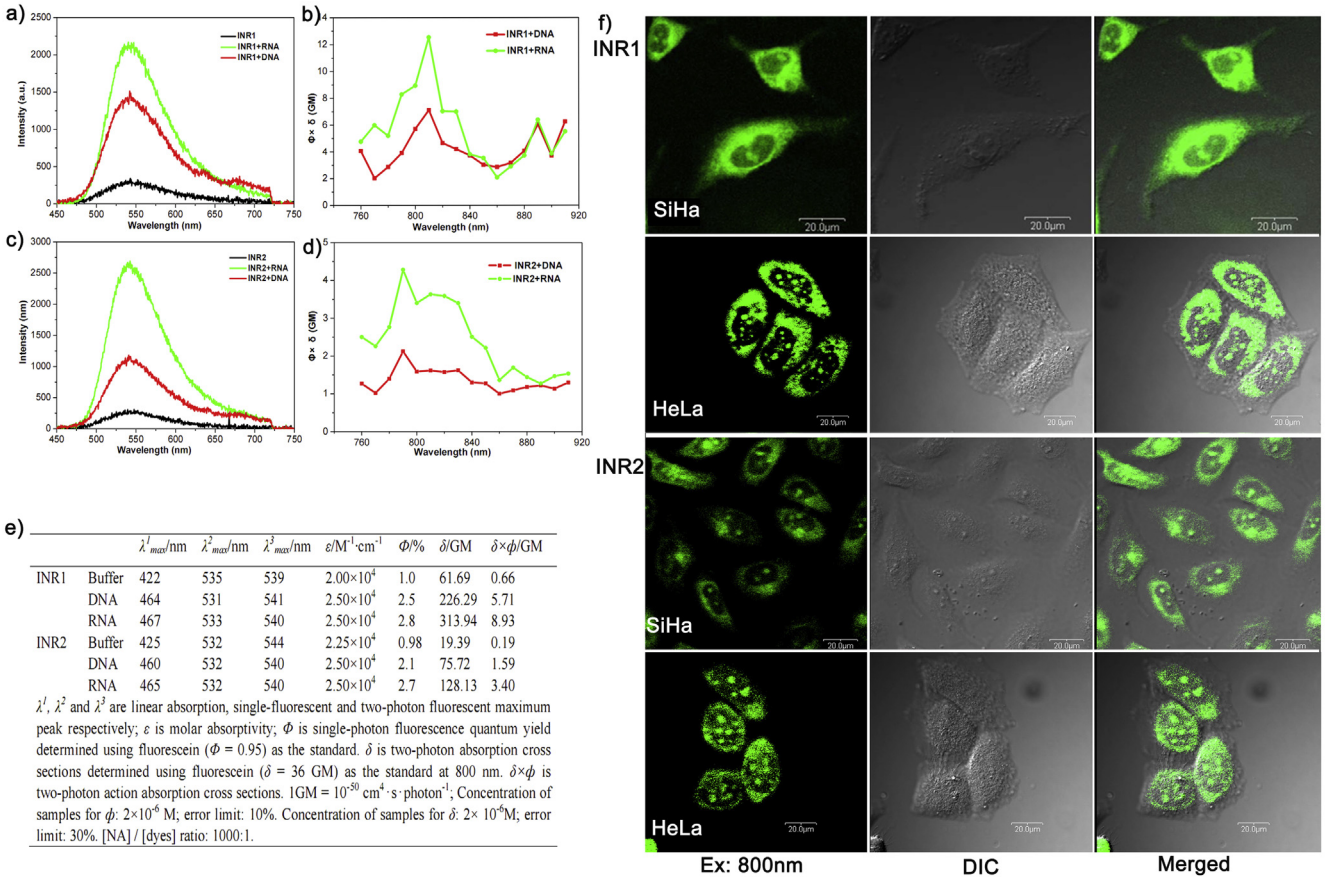

e)

		λ^1_{max}/nm	λ^2_{max}/nm	λ^3_{max}/nm	ε/M^{-1}·cm^{-1}	Φ/%	δ/GM	$\delta\times\phi$/GM
INR1	Buffer	422	535	539	2.00×10^4	1.0	61.69	0.66
	DNA	464	531	541	2.50×10^4	2.5	226.29	5.71
	RNA	467	533	540	2.50×10^4	2.8	313.94	8.93
INR2	Buffer	425	532	544	2.25×10^4	0.98	19.39	0.19
	DNA	460	532	540	2.50×10^4	2.1	75.72	1.59
	RNA	465	532	540	2.50×10^4	2.7	128.13	3.40

λ^1, λ^2 and λ^3 are linear absorption, single-fluorescent and two-photon fluorescent maximum peak respectively; ε is molar absorptivity; Φ is single-photon fluorescence quantum yield determined using fluorescein (Φ = 0.95) as the standard. δ is two-photon absorption cross sections determined using fluorescein (δ = 36 GM) as the standard at 800 nm. $\delta\times\phi$ is two-photon action absorption cross sections. 1GM = 10^{-50} cm^4·s·photon^{-1}; Concentration of samples for ϕ: 2×10^{-6} M; error limit: 10%. Concentration of samples for δ: 2×10^{-6}M; error limit: 30%. [NA] / [dyes] ratio: 1000:1.

Fig. 7. Two-photon photophysical properties and fluorescent images of **INR1**/**INR2**. a and c: Two-photon excited fluorescence spectra of dyes in the absence and in the presence of DNA or RNA. Error limit: 8%. b and d: Two-photon action absorption spectra of dyes in DNA and RNA; Error limit: 20%. f: TPM fluorescence images of live-cells (SiHa and HeLa) stained with 10 μM dyes for 1.5 h. Compound concentration: 2.0 μM. Ratio (phosphate of NA/dye): 1000:1 for **INR1**/**INR2**. Ex: 800 nm, Bar = 20 μm.

TPM. As was revealed from the absorption experiments, the linear absorption wavelengths of **INR1** + RNA and **INR2** + DNA are in the range of 350–500 nm, hence their two-photon absorption experiments can be excited by a sapphire laser source, Ti, which emits lights with the wavelength of 760–910 nm. Moreover, the TPEF of **INR1** + RNA is far higher than that of **INR1**, and is significantly stronger than **INR1** + DNA. The intensity of **INR1** + RNA at 540 nm is 9 times as strong as that of **INR1** at the same wavelength (Fig. 7a). The corresponding ratio of **INR2** + RNA is 11 (Fig. 7c). From Figs. 7b and d, the maximum $\Phi \times \delta$ of **INR1**/**INR2** in DNA and RNA solutions are at approximate 800 nm. $\Phi \times \delta$ of **INR1** in the presence of DNA and RNA are 7.11 GM and 12.53 GM at 810 nm, much larger $\Phi \times \delta$ in comparison with commercial NA dyes, such as DAPI-DNA (2.18 GM) [22] and EBDNA (0.91 GM) [43]. According to our data, the $\Phi \times \delta$ of **INR1** at 800 nm is 0.66, 5.71 and 8.93 GM in tris–HCl buffer, DNA and RNA, respectively (Fig. 7e) which suggests a *ca.* 8- and 13-fold enhancement compared with that in tris–HCl buffer. Similarly, the $\Phi \times \delta$ of **INR2** in presence of RNA shows *ca.* 14-fold enhancement. These all serve as evidence that the dyes can be used as two-photon fluorescence "light-switch" for RNA.

The TPEF imaging of **INR1**/**INR2** (Fig. 7f) was completed at excitation wavelength 800 nm, and the bright fluorescence was

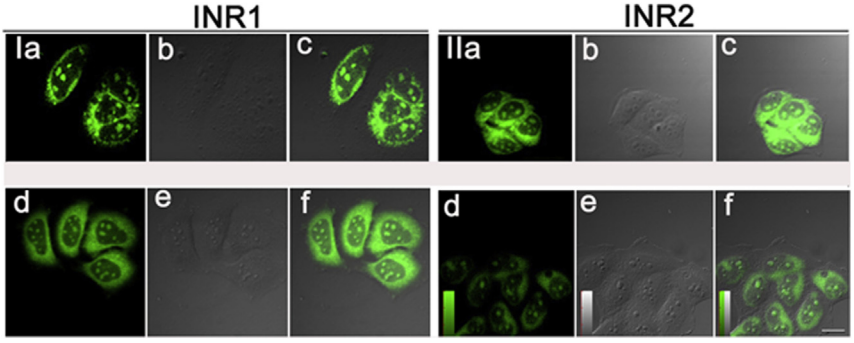

Fig. 8. Two-photon I and II (a–c) and confocal fluorescence I and II (d–f) images of Prefixed cells (HeLa). Cells stained with 5 μM dyes for 30 min. Ex (TP): 800 nm; Ex (confocal fluorescence): 488 nm; Detection wavelength: 510–540 nm; Bar = 20 μm.

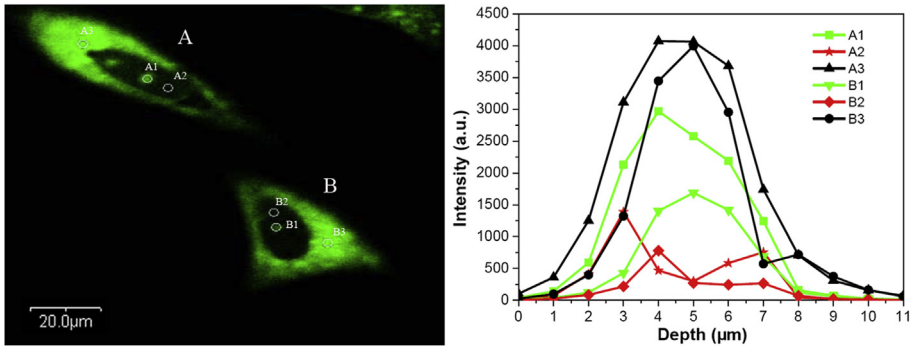

Fig. 9. The left picture: the optical section from video S1. A1 and B1: two areas of nucleoli; A2 and B2: two areas of dark nuclear; A3 and B3: two areas of cytoplasm. A and B stand for the two cells, respectively. The right picture: changes of fluorescence intensity of **INR1** in cell A and B with depths at the same incident power. Red, green and black lines correspond to nuclei nucleoli and cytoplasm, respectively. A1, A2, A3: A; B1, B2, B3: B. (For interpretation of the references to color in this figure legend, the reader is referred to the web version of this article.)

found localized in nucleoli and cytoplasm in different cell types, although different areas exhibit disparity of fluorescent intensity. Consistent with results in confocal microscopy and TPM, **INR1** exhibits better imaging performances than **INR2**. Additionally, according to one- and two-photon bio-imaging (Fig. 8), fixed cells show more nucleoli with significantly different distribution compared to that of living cells, which reflect the difference of RNA dynamics between live-cells and prefixed cells. Furthermore, a video of confocal microscopic imaging of **INR1** including 12 optical sections under the same imaging conditions at different depths has been recorded (see Video S1). In the 12 sections, we randomly selected two nucleoli areas (A1 and B1), two dark nuclear areas (A2 and B2) and two cytoplasm areas (A3 and B3) (Fig. 9). For identical measurement area, the relationship between the fluorescent intensity of **INR1** and imaging depths were plotted in the right picture of Fig. 9 (cell A and B), in which from 0 to 11 μm, fluorescence intensity in nucleoli (A1 and B1) and cytoplasm (A3 and B3) increases dramatically with the increase of depth and then decreases to nearly zero in deeper section, and there is hardly any fluorescence in nuclear area. Fluorescence signal may reveal RNA distribution in nucleoli, the sites of rRNA synthesis, and cytoplasm (rRNA, mRNA and tRNA).

Supplementary video related to this article can be found at http://dx.doi.org/10.1016/j.dyepig.2013.12.005.

3.6. The advantages of *INR1*/*INR2*

First, we have confirmed that the dyes **INR1**/**INR2** can achieve one- and two-photon fluorescence imaging by means of 488 and 800 nm through the above one- and two-photon imaging experiments. Compared to **INR1**/**INR2**, commercially available RNA probe SYTO RNA-Select cannot realize TP fluorescence imaging in living and fixed cells at 800 nm (Fig. S4), and one-photon images with

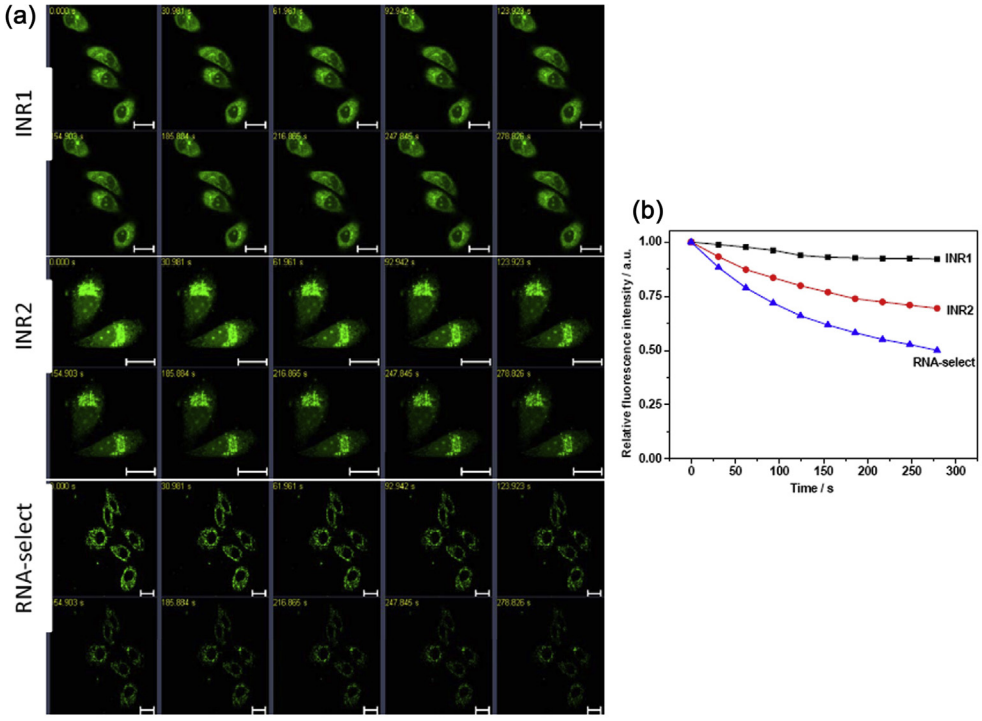

Fig. 10. Comparison of photobleaching of **INR1**/**INR2** and SYTO RNA-Select in confocal fluorescence microscopy imaging. Cells stained with 10 μM dyes for 1.5 h (**INR1**/**INR2**) and 1 μM dyes for 30 min (SYTO RNA-Select); Ex: 488 nm; Detection wavelength: 510–540 nm; Bar = 20 μm.

INR1/**INR2** are more distinct than that with SYTO RNA-Select in living cells (Fig. 10a).

Second, under the high-intensity illumination conditions used for fluorescence microscopy, the irreversible destruction of the excited fluorophore (photobleaching) often becomes the factor limiting fluorescence detectability. Thus, photostability is one of the most important criteria for developing fluorescent imaging agents. Continuous scanning by confocal microscope (Zeiss laser scanning confocal microscope LSM780) was used to quantitatively investigate the photostability of **INR1**/**INR2** and SYTO RNA-Select. Two dishes of SiHa cells subcultured from the same source were stained with 10 μM **INR1**/**INR2** for 1.5 h and 1 μM SYTO RNA-Select for 30 min (According to technology of Molecular Probes Co), respectively. With the help of a power meter, excitation power from 488 nm laser line of the microscope was unified at 60 μW and used to irradiate the **INR1**/**INR2** and SYTO RNA-Select. Within 300 s, the fluorescence signals of **INR1** and **INR2** decreased ~8% and 28%, respectively. In contrast, SYTO RNA-Select exhibited significant photobleaching with only ~45% signal intensity remaining (Fig. 10b). The results indicate that under the applied conditions **INR1**/**INR2** display a much better photostability than SYTO RNA-Select.

4. Conclusions

In summary, two low-molecular-weight fluorescent probes (**INR1**/**INR2**) for detection of RNA in living cells are presented. The two dyes with reasonably large $\Phi \times \delta$ when binding to RNA could be applied to imaging studies with confocal microscopy and TPM. Moreover, they have good counterstain compatibility with Hoechst 33342, which is suitable for RNA–DNA colocalization. Especially, **INR1** has tangible potential as an effective one- and two-photon RNA probes for living cells and we hope this would help the exploitation of novel TPEF probes for RNA. In this study, an important unresolved issue we are hammering at is the lack of specificity of our probe system to specifically monitor particular RNA (e.g., mRNA or rRNA), this area remains under active investigation.

Acknowledgments

For financial support, we thank the National Natural Science Foundation of China (51273107, 30771091, 50990061 and 50721002), Natural Science Foundation of Shandong Province, China (ZR2012EMZ001), Shandong University 2011JC006, Open Project of State Key Laboratory for Supramolecular Structure and Materials (SKLSSM201207).

Appendix A. Supplementary data

Supplementary data related to this article can be found online at http://dx.doi.org/10.1016/j.dyepig.2013.12.005.

References

[1] Zheng M, Librizzi D, Kılıç A, Liu Y, Renz H, Merkel OM, et al. Enhancing in vivo circulation and siRNA delivery with biodegradable polyethylenimine-graftpolycaprolactone-block-poly(ethylene glycol) copolymers. Biomaterials 2012;33:6551–8.
[2] Braasch DA, Jensen S, Liu Y, Kaur K, Arar K, White MA, et al. RNA interference in mammalian cells by chemically-modified RNA. Biochemistry 2003;42:7967–75.
[3] Knowles RB, Sabry JH, Martone ME, Deerinck TJ, Ellisman MH, Bassell GJ, et al. Translocation of RNA granules in living neurons. J Neurosci 1996;16:7812–20.
[4] Cervantes S, Prudhomme J, Carter D, Gopi KG, Li Q, Chang YT, et al. High-content live cell imaging with RNA probes: advancements in high throughput antimalarial drug discovery. BMC Cell Biol 2009;10:45–54.
[5] Honcharenko D, Zhou C, Chattopadhyaya J. Modulation of pyrene fluorescence in DNA probes depends upon the nature of the conformationally restricted nucleotide. J Org Chem 2008;73:2829–42.
[6] Alabi CA, Love KT, Sahay G, Stutzman T, Young WT, Langer R, et al. FRET-labeled siRNA probes for tracking assembly and disassembly of siRNA nanocomplexes. ACS Nano 2012;6:6133–41.
[7] Kam Y, Rubinstein A, Nissan A, Halle D, Yavin E. Detection of endogenous K-ras mRNA in living cells at a single base resolution by a PNA molecular beacon. Mol Pharm 2012;9:685–93.
[8] Santangelo PJ, Nix B, Tsourkas A, Bao G. Dual FRET molecular beacons for mRNA detection in living cells. Nucleic Acids Res 2004;32:e57.
[9] Sando S, Kool ET. Imaging of RNA in bacteria with self-ligating quenched probes. J Am Chem Soc 2002;124:9686–7.
[10] Paige JS, Wu KY, Jaffrey SR. RNA mimics of green fluorescent protein. Science 2011;333:642–5.
[11] Bann DV, Parent LJ. Application of live-cell RNA imaging techniques to the study of retroviral RNA trafficking. Viruses 2012;4:963–79.
[12] Bao G, Rhee1 WJ, Tsourkas A. Fluorescent probes for live-cell RNA detection. Annu Rev Biomed Eng 2009;11:25–47.
[13] Kubota T, Ikeda1 S, Yanagisawa H, Yuki M, Okamoto A. Sets of RNA repeated tags and hybridization-sensitive fluorescent probes for distinct images of RNA in a living cell. PLoS One 2010;9:e13003.
[14] Catrina IE, Marras SAE, Bratu DP. Tiny molecular beacons: LNA/2-O-methyl RNA chimeric probes for imaging dynamic mRNA processes in living cells. ACS Chem Biol 2012;7:1586–95.
[15] Santangelo P, Nitin N, Bao G. Nanostructured probes for RNA detection in living cells. Ann Biomed Eng 2006;34:39–50.
[16] Krishan A, Dandekar PD. DAPI fluorescence in nuclei isolated from tumors. J Histochem Cytochem 2005;53:1033–6.
[17] Pendergrass W, Wolf N, Poot M. Efficacy of MitoTracker Green™ and CMXrosamine to measure changes in mitochondrial membrane potentials in living cells and tissues. Cytom A 2004;61:162–9.
[18] Yu J, Parker D, Pal R, Poole RA, Cann MJ. A europium complex that selectively stains nucleoli of cells. J Am Chem Soc 2006;128:2294–9.
[19] Kumar CV, Asuncion EH. DNA binding studies and site selective fluorescence sensitization of an anthryl probe. J Am Chem Soc 1993;115:8541–53.
[20] Li Q, Kim Y, Namm J, Kulkarni A, Rosania GR, Ahn YH, et al. RNA-selective, live cell imaging probes for studying nuclear structure and function. Chem Biol 2006;13:615–23.
[21] Haugland RP. In: Spence MTZ, editor. A guide to fluorescent and labeling technologies: the handbook. 10th ed. 2005. pp. 710–1.
[22] Li L, Shen X, Xu Q-H, Yao SQ. A switchable two-photon membrane tracer capable of imaging membrane-associated protein tyrosine phosphatase activities. Angew Chem Int Ed Engl 2013;52:424–8.
[23] Oheim M, Michael DJ, Geisbauer M, Madsen D, Chow RH. Principles of two-photon excitation fluorescence microscopy and other nonlinear imaging approaches. Adv Drug Deliv Rev 2006;58:788–808.
[24] Dedov VN, Coxb GC, Roufogalis BD. Visualisation of mitochondria in living neurons with single- and two-photon fluorescence laser microscopy. Micron 2001;32:653–60.
[25] Cho EE, Drazic J, Ganguly M, Stefanovic B, Hynynen K. Two-photon fluorescence microscopy study of cerebrovascular dynamics in ultrasound-induced blood-brain barrier opening 2011;31:1852–62.
[26] Hoptand A, Neher E. Highly nonlinear photodamage in two-photon fluorescence microscopy. Biophys J 2001;80:2029–36.
[27] Potter SM. Vital imaging: two photons are better than one. Curr Biol 1996;6:1595–8.
[28] Li C, Liu Y, Wu Y, Sun Y, Li F. The cellular uptake and localization of non-emissive iridium(III) complexes as cellular reaction-based luminescence probes. Biomaterials 2013;34:1223–34.
[29] Patterson GH, Piston DW. Photobleaching in two-photon excitation microscopy. Biophys J 2000;78:2159–62.
[30] van Zandvoort MAMJ, de Grauw CJ, Gerritsen HC, Broers JLV, oude Egbrink MGA, Ramaekers FCS, et al. Discrimination of DNA and RNA in cells by a vital fluorescent probe: life time imaging of SYTO13 in healthy and apoptotic cells. Cytometry 2002;47:226–35.
[31] Zhang M, Yu M, Li F, Zhu M, Li M, Gao Y, et al. A highly selective fluorescence turn-on sensor for cysteine/homocysteine and its application in bioimaging. J Am Chem Soc 2007;129:10322–3.
[32] Lee JH, Lim CS, Tian YS, Han JH, Cho BR. A two-photon fluorescent probe for thiols in live cells and tissues. J Am Chem Soc 2010;132:1216–7.
[33] Koo CK, Wong KL, Man CWY, Tam HL, Tsao SW, Cheah KW, et al. Two-photon plasma membrane imaging in live cells by an amphiphilic, water-soluble cyctometalated platinum(II) complex. Inorg Chem 2009;48:7501–3.
[34] Gaus K, Gratton E, Kable EPW, Jones AS, Gelissen I, Kritharides L, et al. Visualizing lipid structure and raft domains in living cells with two-photon microscopy. Proc Natl Acad Sci U S A 2003;100:15554–9.
[35] Yang Z, Zhao N, Sun Y, Miao F, Liu Y, Yu X, et al. Highly selective red- and green-emitting two-photon fluorescent probes for cysteine detection and their bio-imaging in living cells. Chem Commun 2012;48:3442–4.
[36] Ohulchanskyy TY, Pudavar HE, Yarmoluk SM, Yashchuk VM, Bergey EJ, Prasad PN. A monomethine cyanine dye cyan 40 for two-photon-excited fluorescence detection of nucleic acids and their visualization in live cells. Photochem Photobiol 2003;77:138–45.

[37] Zhang Y, Wang J, Jia P, Yu X, Liu H, Liu X, et al. Two-photon fluorescence imaging of DNA in living plant turbid tissue with carbazole dicationic salt. Org Biomol Chem 2010;8:4582–8.
[38] Miao F, Song G, Sun Y, Liu Y, Guo F, Zhang W, et al. Fluorescent imaging of acidic compartments in living cells with a high selective novel one-photon ratiometric and two-photon acidic pH probe. Biosens Bioelectron 2013;50:42–9.
[39] Liu X, Sun Y, Zhang Y, Miao F, Wang G, Yu X, et al. A 2, 7-carbazole-based dicationic salt for fluorescence detection of nucleic acids and two-photon fluorescence imaging of RNA in nucleoli and cytoplasm. Org Biomol Chem 2011;9:3615–8.
[40] Xu C, Webb WW. Measurement of two-photon excitation cross sections of molecular fluorophores with data from 690 to 1050 nm. J Opt Soc Am B 1996;13:481–91.
[41] Albota MA, Xu C, Webb WW. Two-photon fluorescence excitation cross sections of biomolecular probes from 690 to 960 nm. Appl Opt 1998;37:7352–6.
[42] Chang C, Chu JF, Kuo H, Kang CC, Lin S, Chang T. Solvent effect on photophysical properties of a fluorescence probe: BMVC. J Luminesc 2006;119:84–90.
[43] Malak H, Castellano FN, Gryczynski I, Lakowicz JR. Two photon excitation of ethidium bromide labeled DNA. Biophys Chem 1997;67:35–41.
[44] Liu X, Sun Y, Zhang Y, Zhao N, Zhao H, Yu X, et al. A series of carbazole cationic compounds with large two-photon absorption cross sections for imaging mitochondria in living cells with two-photon fluorescence microscopy. J Fluoresc 2011;21:497–506.
[45] Hong Y, Lama JWY, Tang BZ. Aggregation-induced emission: phenomenon, mechanism and applications. Chem Commun 2009;29:4332–53.
[46] Lyng R, Hard T, Norden B. Induced CD of DNA intercalators: electric dipole allowed transitions. Biopolymers 1987;26:1327–45.
[47] Larsson A, Carlsson C, Jonsson M, Albinsson B. Characterization of the binding of the fluorescent dyes YO and YOYO to DNA by polarized light spectroscopy. J Am Chem Soc 1994;116:8459–65.